

Estimate of entropy generation rate can spatiotemporally resolve the active nature of cell flickering

Sreekanth K Manikandan,^{1,*} Tanmoy Ghosh,² Tithi Mandal,²
Arikta Biswas,^{2,3} Bidisha Sinha,^{2,†} and Dhrubaditya Mitra^{1,‡}

¹NORDITA, KTH Royal Institute of Technology and Stockholm University, Roslagstullsbacken 23, 10691 Stockholm, Sweden

²Department of Biological Sciences, Indian Institute of Science

Education and Research Kolkata, Mohanpur, Nadia – 741246, India

³Present address: Mechanobiology Institute, National University of Singapore, 5A Engineering Drive, Singapore 117411

We use the short-time inference scheme (Manikandan, Gupta, and Krishnamurthy, *Phys. Rev. Lett.* **124**, 120603, 2020.), obtained within the framework of stochastic thermodynamics, to infer a lower-bound to entropy generation rate from flickering data generated by Interference Reflection Microscopy of HeLa cells. We can clearly distinguish active cell membranes from their ATP depleted selves and even spatio-temporally resolve activity down to the scale of about one μm . Our estimate of activity is *model-independent*.

At the dawn of biophysical research [1], it was already realized that the fundamental property of living cells is that they are not in thermal equilibrium even when they are statistically stationary – they consume energy and generate entropy, see e.g., Ref. [2] for a recent review. Nevertheless, tools of equilibrium physics are frequently used to interpret results of experiments on living cells, for example, equilibrium models are used to infer bending rigidity from flickering data – vibrating fluctuations of a cell membrane, see e.g., Ref. [3] for this and several other examples. Although possible influence of active transport on flickering was first pointed at least seventy years ago [4] investigation into the essential non-equilibrium feature of flickering, by comparing flickering data from a healthy cells with its ATP (adenosine triphosphate)-depleted self, has peaked in the last two decades [5–8], see also Ref [9] and references therein. For RBCs (Red Blood Cells) the first unequivocal demonstration of non-equilibrium nature of flickering was by showing the violation of the fluctuation-dissipation theorem [8]. However no attempt has been made so far to calculate, from flickering data, the fundamental physical quantity that characterises non-equilibrium, v.i.z., the rate of entropy generation, σ .

On one hand, recent spectacular progress in visualizing and tracking biological processes [10–14], with unprecedented accuracy and control, raises hopes that measuring entropy generation rate for cellular processes is indeed possible. On the other hand, there are several difficulties: (a) They are microscopic, lies below the threshold of detection for the existing calorimetric techniques [15]. (b) Thermal fluctuations cannot be ignored, hence any measurement results in noisy readings [16]. (c) Typically we have access to only a few degrees of freedom, e.g., flickering gives us access to the fluctuations of the cell membrane down to a certain length and time scale while

fluctuations at smaller length and time scales and the motion of the cytoskeleton, that drives flickering, are not accessible. (d) In far-from-equilibrium regimes there are very few general principles.

The theoretical understanding of far-from-equilibrium behavior of microscopic systems has undergone a revolution over the last two decades [17, 18] giving rise to the subfield of statistical physics called *Stochastic thermodynamics*, which can in-principle extract entropy generation rate from long-enough stochastic trajectories of *all the degrees of freedoms* of the system [18, 19]. With limited data – limited in both time and number of accessible degrees of freedom – the best we can do is to set bounds [20–32].

In this paper, we use a recent addition to this list of techniques, *the short-time inference scheme* [29], together with flickering data of HeLa cells to estimate spatio-temporally resolved entropy generation rate. As the entropy generation rate is the fundamental characteristic of the active nature of the fluctuations, in the rest of this paper we shall use the word activity and entropy generation rate interchangeably.

The short-time inference scheme is built on the thermodynamic uncertainty relation [22] which states that a lower bound to the entropy generation rate can be obtained via fluctuations of any arbitrary current J in phase space, as,

$$\sigma \geq 2k_B \frac{\langle J \rangle^2}{t \text{Var}(J)}. \quad (1)$$

where $\langle \cdot \rangle$, and $\text{Var}(\cdot)$ denotes mean and variance of a random variable calculated from a statistically stationary time-series of length t and k_B is the Boltzmann constant. Refs. [29, 34, 35] extended this result to show that for a large class of non-equilibrium systems with an overdamped, diffusive dynamics, the inequality, (1), saturates in the short time limit, i.e.,

$$\sigma = 2k_B \lim_{\Delta t \rightarrow 0} \max_J \left[\frac{\langle J_{\Delta t} \rangle^2}{\Delta t \text{Var}(J_{\Delta t})} \right]. \quad (2)$$

* sreekanth.km@fysik.su.se

† bidisha.sinha@iiserkol.ac.in

‡ dhruba.mitra@gmail.com

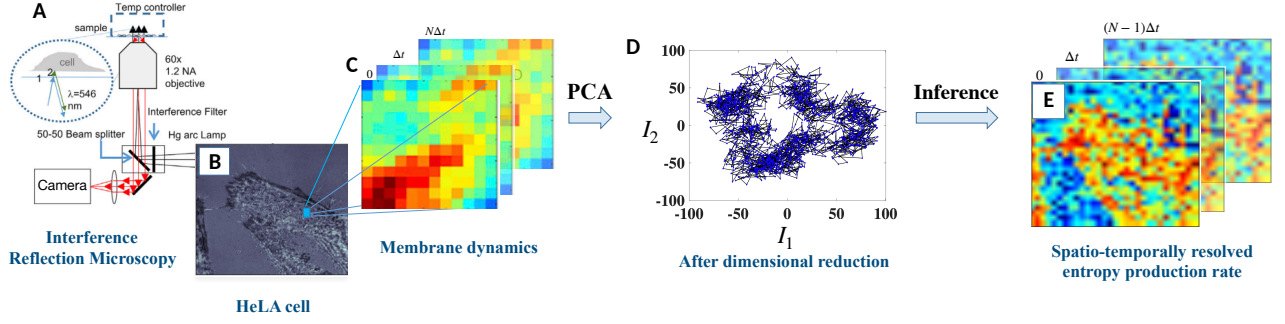


FIG. 1. We use Interference reflection microscopy (A) to obtain flickering data for HeLa cells, representative image in (B) with a patch marked by a sky blue square. Zoomed in picture of the patch in (C) typically contains $M^2 = 400$ pixels. The 400 timeseries are dimensionally reduced to a few (typically 2) by Principal Component Analysis (PCA) (D) The stochastic trajectory of the first two principal components for a typical case. We obtain the entropy production rate, σ by numerical optimisation of this reduced problem. Using the first six principal components instead of the first two has negligible effect on our results. Colormap of σ in (E) clearly shows the active cells compared to its background. The sketch in (A) is adapted from Ref. [33].

Here $J_{\Delta t}$ is calculated over time Δt and the mean and the variance are calculated over an ensemble of such time-intervals.

This scheme has two principal advantages over its competitors: one, it is model independent; two, it is not limited to stationary time-series. This scheme has been successfully used to estimate entropy from a moderate number of realizations of stochastic trajectories of time-dependent systems [31]. In a recent work, the scheme was experimentally tested using the stationary trajectories of a colloidal particle in an stochastically-shaken optical trap [36].

Here we apply Eq. (2) to analyze flickering data from living cell membranes. In Fig. (1) we pictorially summarise our method. We obtain a movie of flickering data for HeLa cells using Interference Reflection Microscopy (IRM), see appendix A1 for details. An example of a cell is shown in Fig. (1B) – in addition to the cell the background is also visible. For the analysis, we divide this cell in $N_p \times M_p$ square patches with N_p and M_p varying between 20–40. One such patch is shown as a blue square in Fig. (1B). Each patch is made of $M \times M$ pixels with $M = 20$. Thus the time evolution of each patch is completely described by M^2 stochastic variables – the light intensity at each of the pixels. The movies are recorded with a time-step $\Delta t = 50$ ms between two consecutive snapshots. A typical movie consists of $N_f = 2048$ snapshots – see Fig. (1C). In order to apply the inference scheme in (2), in principle, we can calculate currents from two consecutive snapshots and average over the number of snapshots to calculate the quantity inside the square brackets in (2). In that case we have to perform numerical optimisation over M^2 space which is quite a formidable problem. Following Ref. [28] we use Principal Component Analysis (PCA) to reduce the dimension of the problem in the following manner. Construct the covariance matrix, of dimension $M^2 \times M^2$ over the complete dataset – this is a real symmetric matrix.

The projection of the data along the eigenfunctions of this covariance matrix considered in decreasing order of eigenvalue are the principal components. We keep only the first two components, $\mathcal{I}_1(t)$ and $\mathcal{I}_2(t)$ – see Fig. (1D). Hence we consider a phase space with dimension $N = 2$. In general, the state of the system is specified by an N dimensional vector $\mathcal{I} = (\mathcal{I}_1, \dots, \mathcal{I}_\alpha, \dots, \mathcal{I}_N)$, e.g., for $N = 2$, $\mathcal{I} = (\mathcal{I}_1, \mathcal{I}_2)$. We define a N dimensional vector $\mathbf{d}(\mathcal{I})$ as a linear combination of the components of \mathcal{I} , i.e.,

$$d_\alpha(\mathcal{I}) = c_{\alpha\beta} \mathcal{I}_\beta, \quad (3)$$

where the matrix $c_{\alpha\beta}$ is a matrix of constant coefficients. At time $t = i\Delta t$ we define a scalar current:

$$J_{\Delta t}(t_i) \equiv \mathbf{d} \left(\frac{\mathcal{I}(t_i + \Delta t) + \mathcal{I}(t_i)}{2} \right) \cdot (\mathcal{I}(t_i + \Delta t) - \mathcal{I}(t_i)) \quad (4)$$

We emphasize that Equation (2) holds for any arbitrarily defined current as long as the vector \mathbf{d} is a smooth function of \mathcal{I} . For simplicity and computational convenience we choose a linear function. Staying within the domain of linear functions, different choices for the matrix elements $c_{\alpha\beta}$ gives different currents. For a fixed choice of $c_{\alpha\beta}$, the mean and the variance of the current are computed by averaging over the index i . Note that this is temporal averaging over a window over which we assume the time-series to be stationary. The method applies equally well for ensemble averaging [31]. The optimisation in (2) is performed using the particle-swarm algorithm [37, 38], as described in Ref. [36]. In Fig. (1E) we plot σ as a pseudocolor for every patch.

In Fig. (2A) we show how our method performs on the experimental data as the cells are ATP-depleted by incubating them in glucose-free ATP-depleting medium. Experimental details are given in section A1b. In the leftmost row we show the image of the cell – the cell boundaries are marked in yellow. The next column shows a pseudocolor plot of the $\ln(\sigma)$ of the live cell – marked

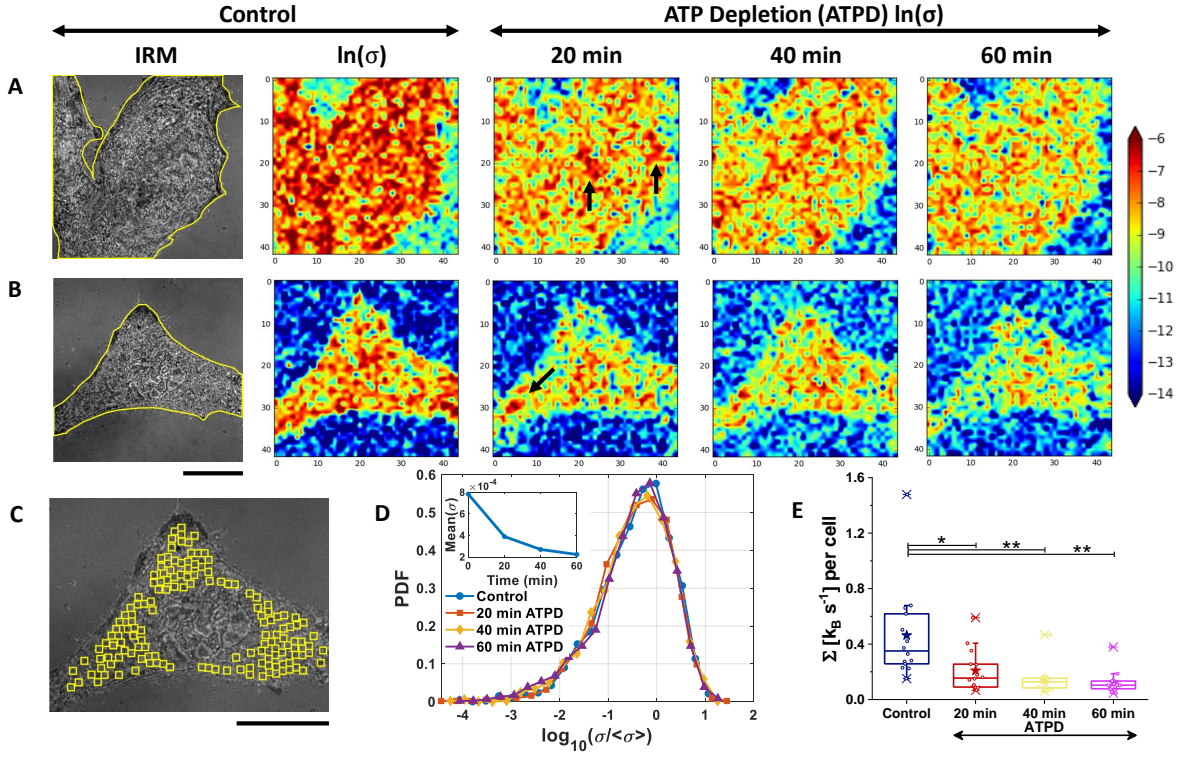


FIG. 2. **Activity of cell membrane.** (A) and (B) From left to right: Typical IRM image of two live HeLa cells – the boundary of the cells are marked in yellow. Colormap of $\ln(\sigma)$ before the cells are treated with ATP-depleting agents. Colormap of $\ln(\sigma)$ after incubating the cells in ATP-depleting agents for 20min., 40min. and 60min. For clarity, the colormap is saturated to -6 . (C) Representative IRM image of a cell with FBRs (size: 20×20 pixels or $1.44 \times 1.44 \mu\text{m}^2$) marked in yellow (D) Probability distribution function of $\log_{10}(\sigma/\langle\sigma\rangle)$, for the FBR-patches, for control and three different durations of ATP-depletion. The four PDFs fall on one another. The inset show the mean value $\langle\sigma\rangle$ for the same four cases. (E) Box plots of activity summed over the FBR-patches. Scale bar = $20 \mu\text{m}$. ** denotes p value < 0.001 and * denotes p value < 0.05 obtained using Mann-Whitney U statistical significance test. Data is from one set of experiments using 14 cells. Two independent repeats show similar trend.

by *control*. The next three columns show how the entropy generation rate changes after 20 minutes, 40 minutes and 1 hr of incubation. In each of these cases we use a movie of $N_f = 2048$ snapshots where consecutive snapshots are separated by $\Delta t = 50 \text{ ms}$. As the total duration of the movie is quite short compared to the time-scales over which ATP-depletion operates, each of these movies are considered statistically stationary. We have performed this experiments for a total 31 HeLa cells, with two independent repeats, from which two typical results are shown here. The plots for the rest of cells are in Appendix A 1. Similar results are obtained in experiments in which the measurements were made after 60 minutes ATP depletion. Our results clearly demonstrate that the entropy production rate computed using (2) spatio-temporally resolves the active nature of cell membrane fluctuations. Notably, we see many patches of high entropy production in the active cell membrane which is well contrasted with the background, and patches of low entropy production in the ATP-depleted membrane, less contrasted with the background. We also see a clear overall decay of σ in time.

To calculate reliable statistical properties of the en-

trophy generation rate, for the control and the ATP-depleted ones – we limit ourselves to patches that are inside the cell and away from the nucleus – an example is shown in Fig. (2B). The relative height of these patches lie within the range $\sim 0 - 100 \text{ nm}$ – termed as first-branch regions (FBRs). Henceforth we call these patches FBR-patches. Henceforth, only the data from the FBR-patches are used to calculate the statistical properties of the entropy generation rate. We plot the probability distribution function (PDF) of $\log_{10}(\sigma/\langle\sigma\rangle)$ from all the FBR-patches of all the cells in Fig. (2C). The PDF for control and all the ATP-depleted cases fall on each other. This suggests that the nature of the PDF remains the same under ATP-depletion, just its mean value $\langle\sigma\rangle$ changes – see the inset of Fig. (2C). The right tail of the PDF is exponential. In Fig. (2D) we show a box-plot the total entropy generation rate of single cells, Σ , obtained summing over all the patches inside the cell boundary. The decrease with time is found to be significant.

Note that the entropy generation rate we calculate is a lower bound of the actual entropy generation rate. Eq. (2) holds when the short-time current $J_{\Delta t}$ includes contributions from all the degrees of freedoms. This is

practically impossible any real physical system. In addition to the necessary coarse-graining which is part of any experimental measurement we coarse-grain the flickering data to include just the first two principal components. We have checked that increasing the number of principal components to six has no significant effect on our results. See Ref. [36] for a longer discussion of the various limitations of our method. Note further that instead of using principal component analysis, we experimented with choosing two random pixels among the M^2 pixels and repeated the analysis. This, quite expectedly, failed to capture the entropy generation rate. We also choose N smallest Fourier modes and repeated the analysis. In this case too, very little difference between active and ATP-depleted cases were observed.

Which cellular processes are the major contributors to the measured activity? Of the many ATP-dependent processes that may actively impact membrane fluctuations, forces originating at the underlying actomyosin cortex are important [39]. The effect of actin polymerizing forces [40] as well as forces by myosin motor protein contracting the actin network are expected to be diminished if the cortex is weakened or even removed. To uncover the contribution of these forces to the measured activity we use the drug Cytochalasin D (Cyto D) that suppresses actin polymerization and weakens the network. It has been shown that as an effect of Cyto D the cortical network is subsequently contracted and fragmented by myosin. The cortex ruptures, clears from most of the membrane area and accumulates as multiple foci [41]. In Fig. (3) we show the effect of cyto-D on the entropy production rate. We find a significant decrease in activity. The decrease is smaller than the decrease measured for ATP depletion and like ATP depletion, the shape of the PDF of σ is preserved while the mean decreases. The data demonstrates that cytoskeleton forces indeed contribute to a fraction of the entropy generated in live cells.

Note that our attempt to tease out the essential non-equilibrium feature from flickering by using the entropy generation rate as a measure of activity has a clear advantage over earlier methods, such as the ones dependent on the breakdown of the fluctuation-dissipation relation e.g. Refs. [8, 42–44]. First, the entropy generation rate is the crucial measure of non-equilibrium – if a system A has a higher entropy generation rate than a system B then A is *further away* from equilibrium than B. Second, we are able to spatiotemporally resolve the entropy generation rate thereby able to identify regions that have higher entropy generation rate than others. Third, our method is model independent estimate of the lower-bound of entropy generation whereas Ref [8] must use a model for active fluctuations. Finally, the measurements in Ref. [8, 42–44] are typically invasive in nature – they involve tracking the response of microscopic beads under external perturbations [11] or attaching fluorescent proteins or filaments to the relevant degrees of freedom [12, 13]. In contrast, our analysis is less invasive and

is applicable to movies made by exploiting the naturally existing intracellular contrast [14].

So far, we have demonstrated, by estimating entropy generation rate from flickering data in a model-independent manner, the active nature of flickering. Let us now consider the following problem. Can we also estimate the time-scale of the active processes that plays the most significant role? Such an estimate is necessarily model dependent.

Usually, flickering data is interpreted with a model [3, 45, 46] of the membrane, in thermal equilibrium at temperature T , described by a height field $h(x, y)$ above the x - y plane. The Hamiltonian in Monge gauge is

$$\mathcal{H}[h] = \int dx dy \left[\frac{\gamma}{2} |\nabla h|^2 + \frac{\kappa}{2} (\nabla^2 h)^2 \right], \quad (5)$$

where we have made the usual assumption of small fluctuations and γ is the tension and κ is the bending rigidity of the membrane. This model or its analog for quasi-spherical vesicles [47] can be solved analytically to solve for the equal-time spectrum of height fluctuations

$$S(\mathbf{q}) \equiv \langle \hat{h}(\mathbf{q}, t) \hat{h}(-\mathbf{q}, t) \rangle, \quad (6)$$

where $\hat{h}(\mathbf{q}, t)$ is the Fourier transform of $h(\mathbf{x}, t)$ and $\langle \cdot \rangle$ denotes averaging over thermal equilibrium, by either using the tools of equilibrium thermodynamics [45, 46] or by turning the problem into a driven dissipative one [47, 48] that satisfies fluctuation-dissipation theorem. The latter also allows calculation of frequency-dependent spectrum [48]. The simplest active models [8, 9, 49–53] add an additional active noise to this model. Unlike the thermal noise, the active noise is not white-in-time but is exponentially-correlated in time. It is supposed to model both on-membrane (e.g., exo and endo cytosol) and cytoskeleton-driven active processes. For such a model, the Fourier modes are uncoupled. Hence the total entropy generation rate is a sum over all \mathbf{q} of entropy generation rate of individual Fourier modes, $\sigma_{\mathbf{q}}$ i.e., $\sigma = \sum \sigma_{\mathbf{q}}$. The contribution from individual Fourier modes can be calculated by a mapping the problem to a well-studied model in stochastic thermodynamics [36, 54, 55]:

$$\sigma_{\mathbf{q}} = \frac{2k_B}{\tau_A(\mathbf{q})} \left[\frac{S(\mathbf{q})|_A}{S(\mathbf{q})|_{\text{Eq}}} - 1 \right], \quad (7)$$

where the suffix “Eq” and the suffix “A” denotes that the average is calculated over the thermodynamic equilibrium and the non-equilibrium stationary state respectively, see A 2 for details. Here $\tau_A(\mathbf{q})$ is the characteristic time-scale of active processes at wavevector \mathbf{q} . Although the expression in (7) is neat, it cannot be reliably used to extract the time-scales τ_A from experimental data due to several reasons. One, experimentally the process of ATP-depletion does not turn off all active processes, hence the equilibrium spectrum in (7) is unknown. Two, in reality, the mechanical properties of the membrane such as

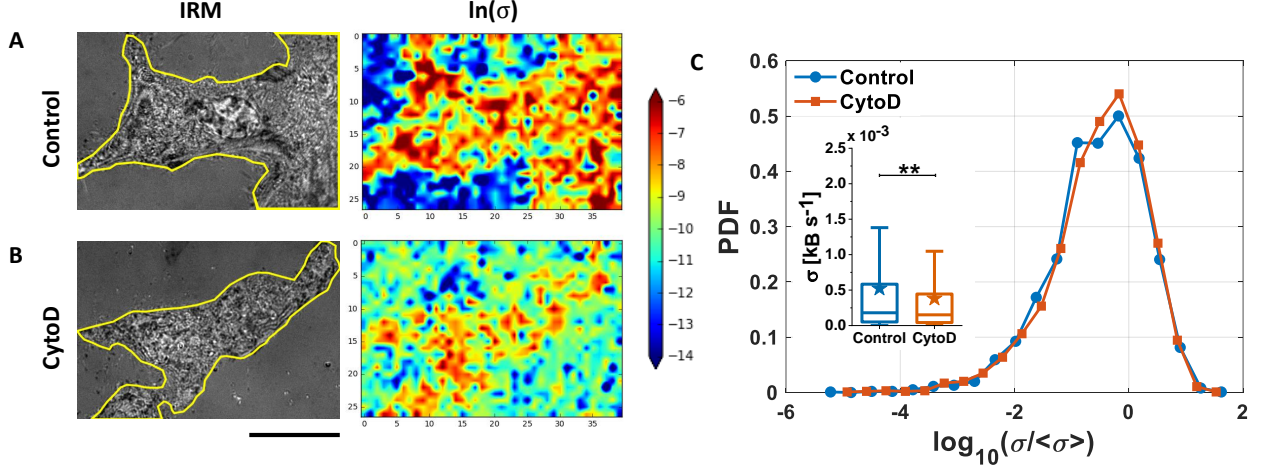


FIG. 3. **How Cyto-D affects activity ?** (A) Irm image and colormap of $\ln(\sigma)$ of a HeLa cell from the control set. (B) Irm image and colormap of $\ln(\sigma)$ of a HeLa cell after Cyto D treatment. Note that unlike Fig. (2) these two are not the same cell. The boundary of the cells are marked in yellow. (C) Probability distribution function of $\log_{10}(\sigma/\langle\sigma\rangle)$, measured from the FBR-patches, for control and after Cyto D treatment. The PDFs fall on one another. The inset compares the σ values using box plots. Here,* denotes the mean, central line denotes the median, upper and lower box edges denote the 75 and 25 percentile respectively. Cyto D treatment reduces σ significantly with a p-value < 0.001 obtained using Mann-Whitney U statistical significance test. Data is representative of three independent experiments on 17 “control” cells and 30 Cyto-D treated ones. The images of all the experiments are in Fig. (6).

σ and κ must also change as a function of ATP depletion [49, 51–53].

Nevertheless, several qualitative conclusions can be drawn. One, the entropy production rate must remain positive hence $S(\mathbf{q})|_A > S(\mathbf{q})|_{Eq}$. As the process of ATP depletion takes the cell membranes closer to the equilibrium state, we expect $S(\mathbf{q})|_A$ to monotonically decrease with ATP-depleting. The total entropy generation rate $\Sigma\sigma(\mathbf{q})$ must converge in the limit of $\mathbf{q} \rightarrow \infty$, this implies that for large $q = |\mathbf{q}|$ the spectrum of fluctuations must approach its equilibrium value. Indeed, we find that fluctuations of the cell membranes we studied experimentally exhibit these qualitative features as shown in Fig. (4). In Fig. (4) we plot $S(\mathbf{q})$ for the two cell samples in Fig. (2). For simplicity, we have only plotted $S(\mathbf{q})$ for $\mathbf{q}[0, i] \equiv q_x$ with $1 \leq i \leq 9$. We find that it decreases as a function of ATP depletion in time for a fixed \mathbf{q} .

In summary, we use a short-time inference scheme to infer entropy generation rate from flickering data. Our scheme allows us to clearly distinguish active cell membranes from ATP depleted ones and to obtain even a spatial map of activity down to the scale of about one μm . We have further verified that our findings qualita-

tively agree with the predictions for a simple model of active membrane. We emphasize that our estimate of activity is *model-independent*.

Measurements that tracked a single filament of microtubules report an entropy production rate of $5k_B \text{ min}^{-1}$ [32] while a single actin fibre contracted by myosin motors report an entropy generation rate, per-unit-length, to be $\sim 1 k_B (\mu\text{ms})^{-1}$ [56]. At the level of cells, calcium flicker trajectories yield $\sim 4 k_B \text{ min}^{-1}$ [32]. Extending such measurements to the cell membranes offer many challenges. First, not one, but multiple active processes with a range of time scales, (timescales: 0.1-2s [8, 33]) act on the membrane and the flickering data does not contain any clearly active “spikes”. Second, the spatial resolution is limited by the diffraction limit of light and the temporal resolution is limited by the signal to noise ratio. Nevertheless, our scheme reveals an activity of $\sim 10^{-3} k_B \text{ s}^{-1}$ over a $1.44 \times 1.44 \mu\text{m}^2$ patch of the membrane. On one hand, this is a extremely small amount of entropy generation rate to detect from calorimetric point of view. On the other hand, summed over all the FBR-patches we obtain $\sim 0.4 k_B \text{ s}^{-1}$ — six-times more than the numbers reported in Ref. [32] who used

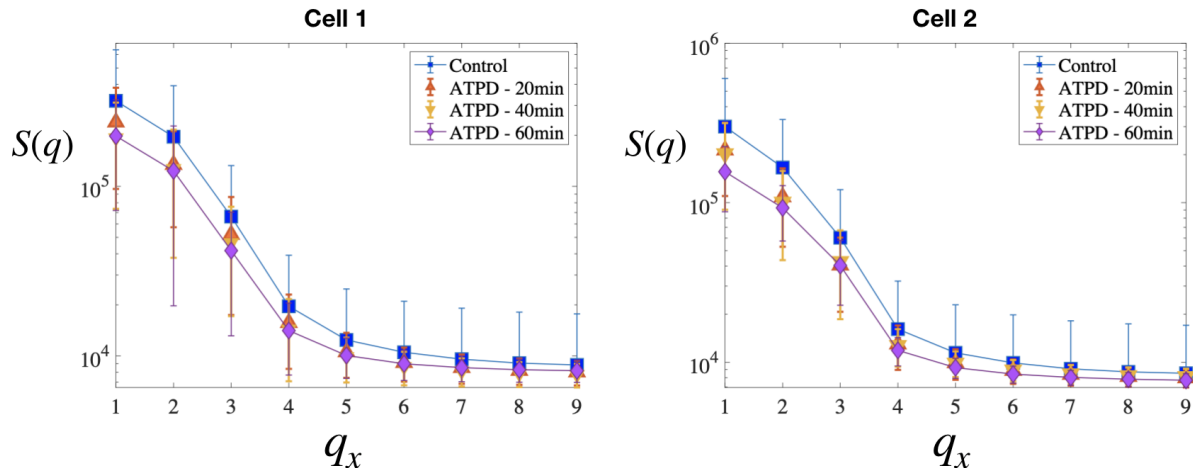


FIG. 4. The spectrum of height fluctuations, $S(q)$, as a function of q in the horizontal direction for the two cells shown in Fig. (2). Different symbols denote different duration of ATP-depletion.

measurements of calcium flicker trajectories from single cells reported in Ref. [57]. Besides capturing the cell-level activity, we report for the first time, a spatial mapping of activity. Images have high activity regions (see arrows, figure 2) which disappear on ATP depletion. This offers an explicit evidence of heterogeneity of activity in the cell membrane pointing to a lack of rapid establishment of an statistically homogeneous (although non-equilibrium) state. At a particular patch, the activity may have contributions from the underlying cytoskeleton as our data also reveals. This technique can be combined with fluorescence imaging of a variety of “active” proteins or structures to measure their localized action. Thus, comparing maps of lateral organization of molecules of interest with activity maps could potentially identify those involved in actively regulating processes like cell migration, endocytosis, and mechano-sensing.

ACKNOWLEDGMENTS

Nordita is partially supported by Nordforsk. DM acknowledges the support of the Swedish Research Council Grant No. 638-2013-9243 and 2016-05225. BS acknowledges support from Wellcome Trust/DBT India Alliance fellowship (grant number IA/I/13/1/500885) and CSRP from CEFIPRA (grant number 6303-1). TG thanks CEFIPRA for scholarship. TM is supported by a predoctoral fellowship from the Council of Scientific and Industrial Research (CSIR), India.

-
- [1] E. Schrödinger, *What is life?: With mind and matter and autobiographical sketches* (Cambridge university press, 2012).
 - [2] F. S. Gnesotto, F. Mura, J. Gladrow, and C. P. Broedersz, Broken detailed balance and non-equilibrium dynamics in living systems: a review, *Reports on Progress in Physics* **81**, 066601 (2018).
 - [3] R. Phillips, J. Kondev, J. Theriot, H. G. Garcia, and N. Orme, *Physical biology of the cell* (Garland Science, 2012).
 - [4] R. Blowers, E. M. Clarkson, and M. Maizels, Flicker phenomenon in human erythrocytes, *The Journal of Physiology* **113**, 228 (1951).
 - [5] S. Tuvia, A. Almagor, A. Bitler, S. Levin, R. Korenstein, and S. Yedgar, Cell membrane fluctuations are regulated by medium macroviscosity: evidence for a metabolic driving force, *Proceedings of the National Academy of Sciences* **94**, 5045 (1997).
 - [6] T. Betz, M. Lenz, J.-F. Joanny, and C. Sykes, ATP-dependent mechanics of red blood cells, *Proceedings of the National Academy of Sciences* **106**, 15320 (2009).
 - [7] R. Rodríguez-García, I. López-Montero, M. Mell, G. Egea, N. S. Gov, and F. Monroy, Direct cytoskeleton forces cause membrane softening in red blood cells, *Biophysical journal* **108**, 2794 (2015).
 - [8] H. Turler, D. A. Fedosov, B. Audoly, T. Auth, N. S. Gov, C. Sykes, J.-F. Joanny, G. Gompper, and T. Betz, Equilibrium physics breakdown reveals the active nature of red blood cell flickering, *Nature physics* **12**, 513 (2016).
 - [9] H. Turler and T. Betz, Unveiling the active nature of living-membrane fluctuations and mechanics, *Annual Review of Condensed Matter Physics* **10**, 213 (2019).
 - [10] V. Ntziachristos, Going deeper than microscopy: the optical imaging frontier in biology, *Nature methods* **7**, 603 (2010).
 - [11] C. P. Brangwynne, G. H. Koenderink, F. C. MacKintosh, and D. A. Weitz, Cytoplasmic diffusion: molecular mo-

- tors mix it up, *Journal of Cell Biology* **183**, 583 (2008).
- [12] R. Yasuda, H. Noji, K. Kinoshita Jr, and M. Yoshida, Fl-
atpase is a highly efficient molecular motor that rotates
with discrete 120 steps, *Cell* **93**, 1117 (1998).
 - [13] R. Pepperkok and J. Ellenberg, High-throughput fluo-
rescence microscopy for systems biology, *Nature reviews*
Molecular cell biology **7**, 690 (2006).
 - [14] Z. Wang, H. Ding, R. Bashir, G. Popescu, L. Millet,
M. Gillette, and V. Chan, Label-free intracellular trans-
port measured by spatial light interference microscopy,
Journal of Biomedical Optics **16**, 026019 (2011).
 - [15] L. Basta, S. Veronesi, Y. Murata, Z. Dubois, N. Mishra,
F. Fabbri, C. Coletti, and S. Heun, A sensitive calori-
metric technique to study energy (heat) exchange at the
nano-scale, *Nanoscale* **10**, 10079 (2018).
 - [16] C. Bustamante, J. Liphardt, and F. Ritort, The nonequi-
librium thermodynamics of small systems, *Physics Today*
58, 43 (2005).
 - [17] C. Jarzynski, Equalities and inequalities: Irreversibility
and the second law of thermodynamics at the nanoscale,
Annu. Rev. Condens. Matter Phys. **2**, 329 (2011).
 - [18] U. Seifert, Stochastic thermodynamics, fluctuation the-
orems and molecular machines, *Reports on progress in*
physics **75**, 126001 (2012).
 - [19] J. M. Parrondo, C. Van den Broeck, and R. Kawai, En-
tropy production and the arrow of time, *New Journal of*
Physics **11**, 073008 (2009).
 - [20] M. Esposito, Stochastic thermodynamics under coarse
graining, *Physical Review E* **85**, 041125 (2012).
 - [21] M. Esposito, Erratum: Stochastic thermodynamics un-
der coarse graining [*phys. rev. e* **85**, 041125 (2012)], *Phys-
ical Review E* **86**, 049904 (2012).
 - [22] A. C. Barato and U. Seifert, Thermodynamic uncertainty
relation for biomolecular processes, *Physical review let-
ters* **114**, 158101 (2015).
 - [23] G. Bisker, M. Poletti, T. R. Gingrich, and J. M.
Horowitz, Hierarchical bounds on entropy production in-
ferred from partial information, *Journal of Statistical Me-
chanics: Theory and Experiment* **2017**, 093210 (2017).
 - [24] I. Lestas, G. Vinnicombe, and J. Paulsson, Fundamen-
tal limits on the suppression of molecular fluctuations,
Nature **467**, 174 (2010).
 - [25] T. R. Gingrich, G. M. Rotskoff, and J. M. Horowitz,
Inferring dissipation from current fluctuations, *Journal*
of Physics A: Mathematical and Theoretical **50**, 184004
(2017).
 - [26] J. M. Horowitz and T. R. Gingrich, Thermodynamic
uncertainty relations constrain non-equilibrium fluctua-
tions, *Nature Physics* **16**, 15 (2020).
 - [27] J. Li, J. M. Horowitz, T. R. Gingrich, and N. Fakhri,
Quantifying dissipation using fluctuating currents, *Nat-
ure communications* **10**, 1 (2019).
 - [28] F. S. Gnesotto, G. Gradziuk, P. Ronceray, and C. P.
Broedersz, Learning the non-equilibrium dynamics of
brownian movies, *Nature communications* **11**, 1 (2020).
 - [29] S. K. Manikandan, D. Gupta, and S. Krishnamurthy, In-
ferring entropy production from short experiments, *Phys-
ical review letters* **124**, 120603 (2020).
 - [30] A. Frishman and P. Ronceray, Learning force fields from
stochastic trajectories, *Physical Review X* **10**, 021009
(2020).
 - [31] S. Otsubo, S. K. Manikandan, T. Sagawa, and S. Krish-
namurthy, Estimating time-dependent entropy produc-
tion from non-equilibrium trajectories, *Communications*
Physics **5**, 1 (2022).
 - [32] D. J. Skinner and J. Dunkel, Improved bounds on entropy
production in living systems, *PNAS* **118** (2021).
 - [33] A. Biswas, A. Alex, and B. Sinha, Mapping cell mem-
brane fluctuations reveals their active regulation and
transient heterogeneities, *Biophysical journal* **113**, 1768
(2017).
 - [34] S. Otsubo, S. Ito, A. Dechant, and T. Sagawa, Esti-
mating entropy production by machine learning of short-
time fluctuating currents, *Physical Review E* **101**, 062106
(2020).
 - [35] T. Van Vu, Y. Hasegawa, *et al.*, Entropy production es-
timation with optimal current, *Physical Review E* **101**,
042138 (2020).
 - [36] S. K. Manikandan, S. Ghosh, A. Kundu, B. Das,
V. Agrawal, D. Mitra, A. Banerjee, and S. Krishna-
murthy, Quantitative analysis of non-equilibrium sys-
tems from short-time experimental data, *Communica-
tions Physics* **4**, 1 (2021).
 - [37] M. R. Bonyadi and Z. Michalewicz, Particle swarm opti-
mization for single objective continuous space problems:
a review, *Evolutionary computation* **25**, 1 (2017).
 - [38] Y. Zhang, S. Wang, and G. Ji, A comprehensive sur-
vey on particle swarm optimization algorithm and its ap-
plications, *Mathematical problems in engineering* **2015**
(2015).
 - [39] D. V. Köster and S. Mayor, Cortical actin and the plasma
membrane: inextricably intertwined, *Current opinion in*
cell biology **38**, 81 (2016).
 - [40] S. Dmitrieff and F. Nédélec, Amplification of actin poly-
merization forces, *The Journal of cell biology* **212**, 763
(2016).
 - [41] M. Schliwa, Action of cytochalasin d on cytoskeletal net-
works, *The Journal of cell biology* **92**, 79 (1982).
 - [42] T. Ariga, M. Tomishige, and D. Mizuno, Nonequilibrium
energetics of molecular motor kinesin, *Physical review*
letters **121**, 218101 (2018).
 - [43] T. Ariga, M. Tomishige, and D. Mizuno, Experimental
and theoretical energetics of walking molecular motors
under fluctuating environments, *Biophysical reviews* **12**,
503 (2020).
 - [44] T. Ariga, K. Tateishi, M. Tomishige, and D. Mizuno,
Noise-induced acceleration of single molecule kinesin-1,
Phys. Rev. Lett. **127**, 178101 (2021).
 - [45] M. Müller, K. Katsov, and M. Schick, Biological and syn-
thetic membranes: What can be learned from a coarse-
grained description?, *Physics Reports* **434**, 113 (2006).
 - [46] S. Safran, *Statistical thermodynamics of surfaces, inter-
faces, and membranes* (CRC Press, 2018).
 - [47] U. Seifert, Fluid membranes in hydrodynamic flow fields:
Formalism and an application to fluctuating quasispher-
ical vesicles in shear flow, *The European Physical Jour-
nal B-Condensed Matter and Complex Systems* **8**, 405
(1999).
 - [48] R. Alert, J. Casademunt, J. Brugués, and P. Sens, Model
for probing membrane-cortex adhesion by micropipette
aspiration and fluctuation spectroscopy, *Biophysical jour-
nal* **108**, 1878 (2015).
 - [49] J. Prost and R. Bruinsma, Shape fluctuations of active
membranes, *EPL (Europhysics Letters)* **33**, 321 (1996).
 - [50] S. Ramaswamy, J. Toner, and J. Prost, Nonequilibrium
fluctuations, traveling waves, and instabilities in active
membranes, *Physical review letters* **84**, 3494 (2000).

- [51] J.-B. Manneville, P. Bassereau, S. Ramaswamy, and J. Prost, Active membrane fluctuations studied by micropipet aspiration, *Physical Review E* **64**, 021908 (2001).
- [52] M. A. Lomholt, Fluctuation spectrum of quasispherical membranes with force-dipole activity, *Physical Review E* **73**, 061914 (2006).
- [53] B. Loubet, U. Seifert, and M. A. Lomholt, Effective tension and fluctuations in active membranes, *Physical Review E* **85**, 031913 (2012).
- [54] A. Pal and S. Sabhapandit, Work fluctuations for a brownian particle in a harmonic trap with fluctuating locations, *Phys. Rev. E* **87**, 022138 (2013).
- [55] S. K. Manikandan and S. Krishnamurthy, Exact results for the finite time thermodynamic uncertainty relation, *Journal of Physics A: Mathematical and Theoretical* **51**, 11LT01 (2018).
- [56] D. S. Seara, V. Yadav, I. Linsmeier, A. P. Tabatabai, P. W. Oakes, S. Tabel, S. Banerjee, and M. P. Murrell, Entropy production rate is maximized in non-contractile actomyosin, *Nature communications* **9**, 1 (2018).
- [57] K. Thurley, S. C. Tovey, G. Moenke, V. L. Prince, A. Meena, A. P. Thomas, A. Skupin, C. W. Taylor, and M. Falcke, Reliable encoding of stimulus intensities within random sequences of intracellular Ca^{2+} spikes, *Science signaling* **7**, ra59 (2014).
- [58] H.-F. Renard, M. Simunovic, J. Lemièrre, E. Boucrot, M. D. Garcia-Castillo, S. Arumugam, V. Chambon, C. Lamaze, C. Wunder, A. K. Kenworthy, *et al.*, Endophilin-a2 functions in membrane scission in clathrin-independent endocytosis, *Nature* **517**, 493 (2015).
- [59] L. Limozin and K. Sengupta, Quantitative reflection interference contrast microscopy (ricm) in soft matter and cell adhesion, *ChemPhysChem* **10**, 2752 (2009).
- [60] S. Chandrasekhar, Stochastic problems in physics and astronomy, *Reviews of modern physics* **15**, 1 (1943).
- [61] C. W. Gardiner, *Handbook of stochastic methods*, Vol. 3 (springer Berlin, 1985).
- [62] L. Dabelow, S. Bo, and R. Eichhorn, Irreversibility in active matter systems: Fluctuation theorem and mutual information, *Physical Review X* **9**, 021009 (2019).
- [63] L. Dabelow and R. Eichhorn, Irreversibility in active matter: General framework for active ornstein-uhlenbeck particles, *Frontiers in Physics* , 516 (2021).
- [64] L. Dabelow, S. Bo, and R. Eichhorn, How irreversible are steady-state trajectories of a trapped active particle?, *Journal of Statistical Mechanics: Theory and Experiment* **2021**, 033216 (2021).
- [65] U. Seifert, Entropy production along a stochastic trajectory and an integral fluctuation theorem, *Physical review letters* **95**, 040602 (2005).
- [66] S. Borlenghi, S. Iubini, S. Lepri, and J. Fransson, Entropy production for complex langevin equations, *Phys. Rev. E* **96**, 012150 (2017).
- [67] A. Argun, J. Soni, L. Dabelow, S. Bo, G. Pesce, R. Eichhorn, and G. Volpe, Experimental realization of a minimal microscopic heat engine, *Phys. Rev. E* **96**, 052106 (2017).
- [68] R. J. Hawkins and T. B. Liverpool, Stress reorganization and response in active solids, *Phys. Rev. Lett.* **113**, 028102 (2014).
- [69] B. Loubet, U. Seifert, and M. A. Lomholt, Effective tension and fluctuations in active membranes, *Phys. Rev. E* **85**, 031913 (2012).

Appendix A: Material and Methods

1. Interference reflection microscopy

a. Cell culture

HeLa cells (CCL-2, ATCC) were grown in Dulbecco's Modified Essential Medium (DMEM, Gibco, Life Technologies, USA) supplemented with 10% foetal bovine serum (FBS, Gibco) and 1% Anti-Anti (Gibco) at $37^{\circ}C$ under 5% CO_2 and $37^{\circ}C$. Experiments were always performed after 16-18 hrs of cell seeding.

b. Pharmacological treatments

Cellular ATP content was depleted by using 10 mM sodium azide and 10 mM 2-deoxy D-glucose are added to cells [58] in M1 Imaging medium (150 mM NaCl; Sigma-Aldrich), 1 mM $MgCl_2$ (Merck, Kenilworth, NJ), and 20 mM HEPES (Sigma-Aldrich) and incubated for 60 min for ATP depletion. For inhibiting actin polymerization, cells were treated with 5 μM cytochalasin D (Cyto D, Sigma Aldrich) for 1 hour in serum free media.

c. IRM Imaging

IRM imaging [33, 59] was performed in a motorized inverted microscope (Nikon, Japan) using adjustable field and aperture diaphragms, 60 \times water immersion objective (NA 1.22), 1.5 \times external magnification, onstage $37^{\circ}C$ incubator (Tokai Hit, Japan), s-CMOS camera (ORCA Flash 4.0, Hamamatsu, Japan), 100 W mercury arc lamp, interference filter (546 ± 12 nm) and a 50-50 beam splitter [33]. For every cell, 2048frames (20 frames/s) were recorded with an exposure time of 50 ms.

d. Analysis of height fluctuations

Pixel intensities were converted to relative height (distance of the membrane from the coverslip) using a MATLAB (MathWorks, USA) code after obtaining the intensity-to-height conversion factor found out by a beads-based calibration method reported previously [33]. Every experiment was preceded by an independent calibration. The height conversion is valid for regions of the basal cell membrane with relative heights lying in the range ~ 0 -100 nm, termed as first-branch regions (FBRs). Although for visual representation, the calibration is applied to every pixel of the image, only the data from the FBRs are used to calculate the statistical properties of the entropy generation rate.

We first measure the height fluctuations before starting ATP-depletion and call it the "Control" condition. At

$t = 0$ we administer the ATP-depleting drugs. We measure the height fluctuations after $t = 20$ min, 40 min. and 1 hr. of incubation. In each of these cases we use a movie of $N_f = 2048$ snapshots where consecutive snapshots are separated by $\Delta t = 50$ ms. From every movie approximately 100–140 FBRs (each of size $\sim 1.44 \times 1.44 \mu\text{m}^2$) were identified and analysed. We use the Mann-Whitney U to test for statistical significance (ns denotes $p > 0.05$, * denotes $p < 0.05$, ** denoted $p < 0.001$).

2. Entropy generation rate in a model of active membrane

We calculate the entropy generation rate for an elementary model of active membrane [49]. Usually, flickering data is interpreted with a model [3, 45, 46] where the membrane is described by a height field $h(x, y)$ above the x - y plane in Monge gauge described by the Hamiltonian

$$\mathcal{H}[h] = \int dx dy \left[\frac{\gamma}{2} |\nabla h|^2 + \frac{\kappa}{2} (\nabla^2 h)^2 \right], \quad (\text{A1})$$

in equilibrium at temperature T . Here γ is the surface tension and κ is the bending rigidity of the membrane. As the fluctuations of h are small, the model uses small deformation approximation of curvature. We shall call this the Gaussian model. The Hamiltonian is diagonal in Fourier space. In the same spirit as Refs. [8, 9, 49] we write an active version of this model by writing an equation of motion for each Fourier mode $\hat{h}(\mathbf{q}, t)$ coupled to an Ornstein-Uhlenbeck noise [60] $\lambda(\mathbf{q}, t)$ as,

$$\frac{\partial \hat{h}(\mathbf{q}, t)}{\partial t} + \frac{1}{\tau(\mathbf{q})} \hat{h}(\mathbf{q}, t) + b \lambda(\mathbf{q}, t) = \sqrt{2D} \zeta(\mathbf{q}, t) \quad (\text{A2a})$$

$$\frac{\partial \lambda(\mathbf{q}, t)}{\partial t} + \frac{1}{\tau_A} \lambda(\mathbf{q}) = \sqrt{2D_A} \zeta_A(\mathbf{q}, t), \quad (\text{A2b})$$

$$\text{where} \quad \tau(\mathbf{q}) = \frac{4\eta q}{\kappa q^4 + \gamma q^2}, \quad (\text{A2c})$$

$$\langle \zeta(\mathbf{q}, t) \zeta(-\mathbf{q}, s) \rangle = 2D(\mathbf{q}) \delta(t - s), \quad (\text{A2d})$$

$$\langle \zeta_A(\mathbf{q}, t) \zeta_A(-\mathbf{q}, s) \rangle = \delta(t - s), \quad \text{and} \quad (\text{A2e})$$

$$D(\mathbf{q}) = \frac{k_B T}{4\eta q} \quad (\text{A2f})$$

The membrane is assumed to undergo stochastically driven overdamped motion. The viscosity of the fluid around the membrane is η which is related to the amplitude of the stochastic driving ζ by fluctuation-dissipation theorem (A2f). In addition, there is active noise, ζ_A which is assumed to be white-in-space and an Ornstein-Uhlenbeck noise (A2b) in time with a correlation time τ_A and an amplitude D_A . This active noise models both active processes on the membrane [49], e.g.,

opening of ion channels, endo and exo cytosol etc, and driving by the cytoskeleton [8]. In (A2a), we use the parameter b (of dimension s^{-1}) to determine the strength of the coupling of the membrane to the active fluctuations. Note that there are other models of time-correlated noises used to model active fluctuations in living systems. In Refs. [8, 9, 49], the active noise is modelled using a random telegraph process [61], which leads to a same exponential correlation in time for the noise as the Ornstein-Uhlenbeck process. In Refs. [62–64] the Ornstein-Uhlenbeck model itself is used.

For simplicity, here onwards, we drop the \mathbf{q} dependence of ζ_A , τ_A , and D_A . As we have ignored nonlinearities in the model for the membrane every $\hat{h}(\mathbf{q})$ is independent of every other $\hat{h}(\mathbf{q})$. Consequently, the total entropy generation rate is a sum over all \mathbf{q} ,

$$\sigma = \sum \sigma_{\mathbf{q}}. \quad (\text{A3})$$

The individual terms in the sum correspond to entropy generation rate for Eqs. A2a and A2b, and can be calculated analytically [65, 66], by mapping to a well-studied model in Stochastic thermodynamics [36, 54, 55]. We obtain,

$$\sigma_{\mathbf{q}} = 2k_B \frac{b^2 D_A \tau(\mathbf{q}) \tau_A}{D(\tau(\mathbf{q}) + \tau_A)}. \quad (\text{A4a})$$

$$= \frac{2k_B}{\tau_A(\mathbf{q})} \left[\frac{S(\mathbf{q})|_A}{S(\mathbf{q})|_{\text{Eq}}} - 1 \right], \quad (\text{A4b})$$

In (A4b) the subscript “A” denotes the variance being calculated for an active membrane ($b \neq 0$) whereas the subscript “Eq” denotes the variance being calculated for membrane in thermal equilibrium – $b = 0$. They can be computed from the knowledge of the stationary distribution of \hat{h} and λ as [54, 67]

$$S(\mathbf{q})|_A = \langle \hat{h}^*(\mathbf{q}) \hat{h}(\mathbf{q}) \rangle = D\tau(\mathbf{q}) + \frac{b^2 D_A \tau(\mathbf{q})^2 \tau_A^2}{\tau + \tau_A}. \quad (\text{A5})$$

We remark that the entropy production rate remains finite in the white noise limit of the Ornstein-Uhlenbeck process.

Notice that, though the model provides an exact analytical expression (8a) and an accessible form (8b) for the entropy production rate, applying it on the experimental data is rather challenging. This is because, we do not have access to either the active time-scale τ_A nor the equilibrium fluctuations of the membrane $S(\mathbf{q})|_{\text{Eq}}$. Furthermore, in reality, the mechanical properties of the membrane such as σ and κ could also change as a function of ATP depletion, and the model practically neglects any such effects [68, 69]. Nevertheless, assuming the model is representative of the actual membrane dynamics observed in the experiments, the following qualitative features can be deduced.

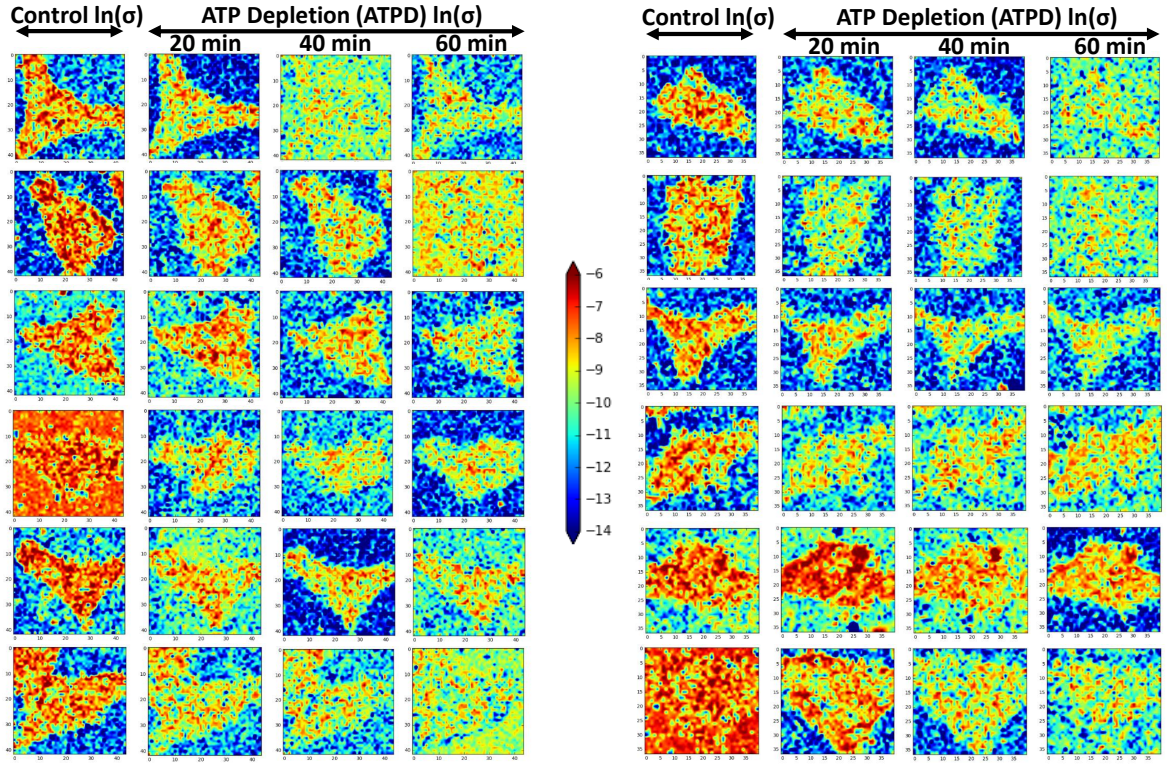


FIG. 5. How ATP-depletion changes the activity map as a function of time for all the cells we have experimented on.

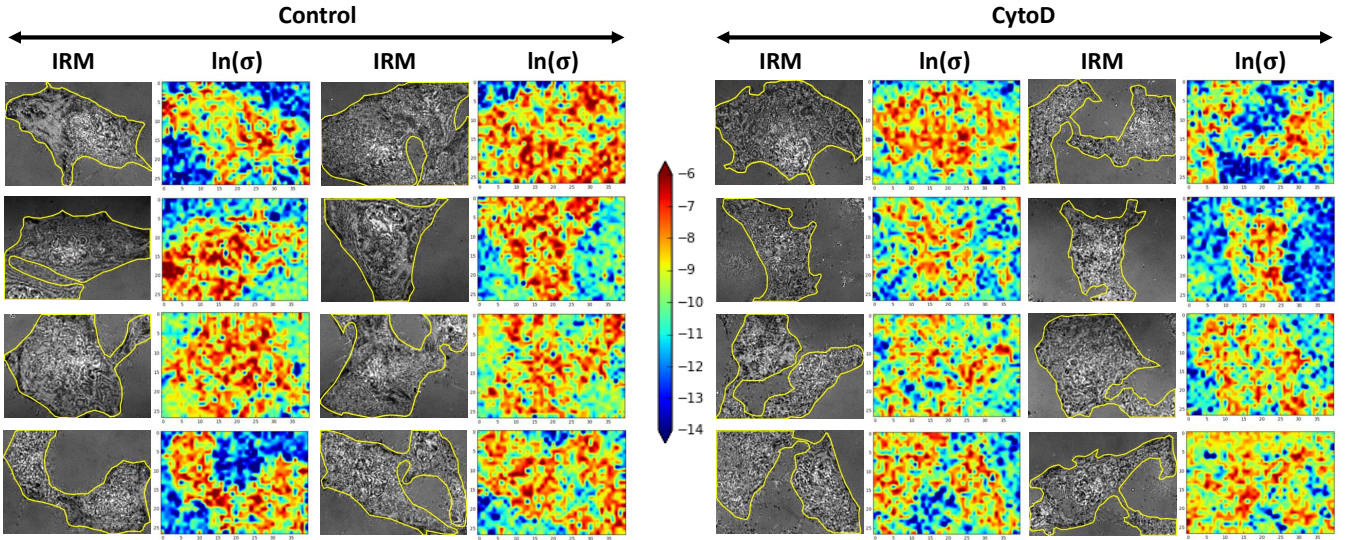


FIG. 6. How treatment with cyto-D changes the activity map as a function of time for all the cells we have experimented on.

1. The entropy production rate vanishes in the $D_A \rightarrow 0$ limit.
2. The entropy production rate must be positive. Hence,

$$S(\mathbf{q})|_A \geq S(\mathbf{q})|_{\text{Eq}} \quad (\text{A6})$$

Assuming that the ATP depletion takes the cell membranes close to the equilibrium state, we can further argue that $S(\mathbf{q})|_A > S(\mathbf{q})|_{\text{ATPD}}$ where the subscript stands for the ATP depleted cell membrane.

3. The summation in Eq. (A3) should converge. Hence,

$$S(\mathbf{q})|_A \rightarrow S(\mathbf{q})|_{\text{Eq}} \text{ for large } q. \quad (\text{A7})$$

As a corollary, we also obtain $S(\mathbf{q})|_A \rightarrow S(\mathbf{q})|_{\text{ATPD}}$ for large q .

Indeed, we find that fluctuations of the cell membranes we studied experimentally exhibit the qualitative features predicted by this model. We summarize our findings in Fig. 4 for the two cell samples in Fig. (2). For simplicity, we have only shown $S(\mathbf{q})|$ for $\mathbf{q}[0, i] \equiv q_x$ with $1 \leq i \leq 9$, and we find that it decreases as a function of ATP depletion in time for a fixed \mathbf{q} .